

## Supporting Information

### **Tumor-Targeting Multi-shelled Hollow Nanospheres as Drug Loading Platforms for Imaging-Guided Combinational Cancer Therapy**

Wentao Wang<sup>a+</sup>, Tao Zheng<sup>a+</sup>, Ming Zhang<sup>a,b\*</sup>, Qicheng Zhang<sup>b</sup>, Fan Wu<sup>b</sup>, Yihan Liu<sup>b</sup>,  
Lin Zhang<sup>c</sup>, Jun Zhang<sup>b</sup>, Mingqian Wang<sup>d\*</sup>, Yi Sun<sup>a\*</sup>

<sup>a</sup>*Department of Health Technology, Technical University of Denmark, Kongens Lyngby, 2800, Denmark;*

<sup>b</sup>*Jiangsu Collaborative Innovation Center for Biomedical Functional Materials, School of Chemistry and Materials Science, Nanjing Normal University, Nanjing 210023, China;*

<sup>c</sup>*Wuxi Children's Hospital, Wuxi, 210023, China;*

<sup>d</sup>*Key Laboratory of High Performance Polymer Material and Technology of Ministry of Education, School of Chemistry and Chemical Engineering, Nanjing University, Nanjing, 210023, China*

*Corresponding authors: Ming Zhang, mzhan@dtu.dk; Mingqian Wang, DG1624064@smail.nju.edu.cn; Yi Sun, suyi@dtu.dk*

<sup>+</sup>These authors contributed equally to this work.

## 1. Experiment section

**1.1 Chemicals.** The following chemicals were purchased and used without further purification: imidazole-2-carboxaldehyde (ICA, 97%, Aladdin), zinc acetate (98%, Aladdin), sodium n-dodecyl sulfate (99%, Alfa Aesar), cetyltrimethylammonium chloride solution (CTAC, 25 wt%, Aldrich), cetyltrimethylammonium bromide (CTAB, 96%, aladdin), dodecyltrimethylammonium bromide (DTAB, 99.9%, Sigma), sodium n-dodecyl sulfate (SDS, 99%, Alfa Aesar), cupric acetylacetonate ( $\text{Cu}(\text{acac})_2$ ,  $\geq 98\%$ , aladdin), tetrabutylammonium borohydride ( $\text{RNBH}_4$ , 98%, Sigma), 1-[3-(dimethylamino) propyl]-3-ethylcarbodiimide hydrochloride (EDC, Sigma), and N-hydroxy-succinimide (NHS, Sigma). The deionized water was obtained from a Milli-Q synthesis system.

All cell lines were provided by the Drum Tower Hospital of Jiangsu Province and cultured with dulbecco's modified eagle medium (DMEM; HyClone), 10 % fetal bovine serum (FBS; GIBCO) and 5%  $\text{CO}_2$  at 37 °C. Methyl thiazolyl tetrazolium (MTT) was purchased from Amresco (USA).

**1.2 Characterization.** The morphology and structure of all the products were characterized by transmission electron microscopy images (TEM, JEM-2100) and X-ray powder diffraction (XRD, Dmax-2500). Fourier transformed infrared (FTIR) spectra were conducted on a Nicolet Nexus 870 FTIR spectrometer (Thermo-Fisher Scientific, USA). The UV-vis absorbance spectra of all the products were obtained using a Shimadzu U-4100 spectrophotometer. The fluorescence emission spectra were recorded using molecular fluorescence spectrometer (Cary Eclipse, Varian, USA), X-ray photoelectron spectroscopy (XPS) analysis was conducted on a PHI 5000 Versa Probe. Fluorescence images were then acquired using a confocal laser scanning microscope (CLSM) (TCS SP5, Leica, Germany).

**1.3 Synthesis of  $a_m$ -ZIF@Cu@Au NPs.** The Synthetic procedure was the similar as the previously reported method by Zhang and co-workers [1]. Briefly, 1.0 mL of  $Zn(NO_3)_2$  aqueous solution (0.3 M) was added to 100 mL DI water. 20 mL of ICA methanolic solution (0.2 M) was added and mixed by vibrating for 2 min. Then, 2 mL of CTAC aqueous solution (3 wt%) was added to the mixture. Usually, the mixture became turbid within 5 min, then it was further stirred for 40 min at 25 °C. The  $a_m$ -ZIF-90 NPs were obtained by removing the large particles through filtering with 0.8- $\mu$ m membranes after 15 min of ultrasound treatment. The final reaction mixture was subjected to wash with 40 mL of ethanol for twice and dried at 60 °C for 12 h.

30 mg of  $a_m$ -ZIF-90 NPs powders were added to 20 mL of methanol by sonication for 10 min. Then,  $Cu(acac)_2$  (1.5 mL) and  $HAuCl_4 \cdot 3H_2O$  (1.5 mL) solution was added under vigorous stirring for 1 h. 2.5 mL of R-NBH<sub>4</sub> solution (125 mM) was added in the mixture. The mixture was continuously stirred for another 30 min. Finally, the product was centrifuged and washed with ethanol for three times, and dried at 60 °C for 12 h. The water-soluble  $a_m$ -ZnO@CuO@Au NPs were obtained.  $a_m$ -ZIF@Cu NPs were synthesized by a method that was similar to the preparation of  $a_m$ -ZIF@Cu@Au NPs, but without  $HAuCl_4 \cdot 3H_2O$ .

**1.4 Calcination of  $a_m$ -ZIF@Cu@Au NPs.** The obtained powders were calcined in a tube furnace with an open hole to contact laboratory air. The operation was the following heating routine: ramping to 280 °C and soaking at 280 °C for 80 min. When cooled down to room temperature, the powders were added to DI water. The  $a_m$ -ZnO@CuO@Au HNSs were obtained by removing the large particles through filtering with 0.65- $\mu$ m membranes after 15 min of ultrasound treatment. The mixture was then sonicated for 10 min and centrifuged (10,000 rpm, 5 min) to collect the  $a_m$ -ZnO@CuO@Au HNSs which were then washed by ethanol for three times and easily dissolved in DI water.  $a_m$ -ZnO NPs and  $a_m$ -ZnO@CuO NPs were synthesized by a method that was similar to the preparation of  $a_m$ -ZnO@CuO@Au HNSs.

**1.5 Synthesis of RGD@*a<sub>m</sub>*-ZnO@CuO@Au HNSs.** *a<sub>m</sub>*-ZnO@CuO@Au HNSs were passivated with PEG-COOH at 100 °C with the presence of nitrogen gas. The excess amount of PEG-COOH was removed by membrane dialysis (MWCO 3000). Then 1-(3-dimethylaminopropyl)-3-ethylcarbodiimide hydrochloride (EDC, 0.2 g) and N-hydroxysuccinimide (NHS, 0.2 g) were introduced to a methanol suspension (150 mL) of *a<sub>m</sub>*-ZnO@CuO@Au@PEG-COOH HNSs (30 mg) to activate the carboxylic acid groups of *a<sub>m</sub>*-ZnO@CuO@Au@PEG HNSs, and the mixture was stirred gently at room temperature for 3 h. Then NH<sub>2</sub>-cRGD (3 mg) was added into above suspension and the reaction was conducted by vigorously stirring at 4 °C for another 6 h under vigorously stirring. After reaction, unreacted cRGD was removed by ultrafiltration. The mixture was further washed with PBS for three times, and then dispersed in PBS.

**1.6 DOX loading and releasing.** RGD@*a<sub>m</sub>*-ZnO@CuO@Au HNSs were incubated with DOX in PBS solution (pH 7.4) for 20 h under dark condition at a certain drug concentration. The DOX-loaded RGD@*a<sub>m</sub>*-ZnO@CuO@Au (RGD@*a<sub>m</sub>*-ZnO@CuO@Au@DOX) were collected by centrifugation and washed for three times with PBS to remove the excess DOX. The supernatant and washed solutions were collected, and the amount of unbound DOX was determined by UV-vis spectroscopy at 490 nm to estimate the drug-loading efficiency.

Red light-simulated release of DOX was carried out by 635 nm laser irradiation. In a typical experiment, the RGD@*a<sub>m</sub>*-ZnO@CuO@Au@DOX HNSs were dissolved in 5 mL PBS solution at different pH values (5.0 and 7.4). At different time points, the samples were irradiated by 635-nm laser for 5 min with the power density of 2.0 W/cm<sup>2</sup>. After the treatment, 500 μL of solution was collected and centrifuged to obtain released DOX, which was determined by UV-Vis-NIR spectrum [2].

**1.7 Electron spin resonance spectroscopy.** All the ESR measurements were carried out by a Bruker EMX ESR spectrometer (Billerica, MA, USA) at ambient

temperature.

The spin trap BMPO was used to verify the formation of •OH during exposure of *a<sub>m</sub>*-ZnO NPs, *a<sub>m</sub>*-ZnO@Au NPs, *a<sub>m</sub>*-ZnO@CuO NPs, and *a<sub>m</sub>*-ZnO@CuO@Au HNSs to simulated red light. 4-Oxo-TEMP was used to demonstrate the generation of <sup>1</sup>O<sub>2</sub> during irradiation of samples. In these experiments, the intensity of the ESR signal was measured as the peak-to-peak height of the second line of ESR spectrum. ESR spectra were recorded from the sample mixture containing spin probes (4-Oxo-TEMP) and *a<sub>m</sub>*-ZnO NPs, *a<sub>m</sub>*-ZnO@Au NPs, *a<sub>m</sub>*-ZnO@CuO NPs, and *a<sub>m</sub>*-ZnO@CuO@Au HNSs, after exposure to simulated red light for selected times. For comparison, controls without either catalysts or irradiation were also recorded. The final concentration of each component was described in each figure caption. NaN<sub>3</sub> was employed to separately test their scavenging effect on the ESR signal for <sup>1</sup>O<sub>2</sub>.

**1.8 Detection of intracellular ROS generation.** Measurements of intracellular total ROS and superoxide anion were performed with dichloro-dihydrofluorescein-diacetate (DCFH-DA) and dihydroethidium (DHE) dyes. In brief, A549 cells were seeded in 6 cm culture plate ( $3 \times 10^5$  cells) and cultured overnight. Cells were treated with *a<sub>m</sub>*-ZnO@CuO@Au HNSs at several concentrations (0, 25, 50, and 100 µg/mL) for 24 h, and then irradiated by 635 nm laser at different power densities (0 or 0.1 W/cm<sup>2</sup>) for 10 min. Subsequently, cells were harvested and incubated with a serum-free DMEM medium containing DCFH-DA (10 µg/mL) and DHE (10 µg/mL) for 20 min. One hundred microliters ( $\sim 2 \times 10^4$  cells per well) of the cell suspension were dispensed into each well of a 96-well black view plate. Fluorescence intensity was quantified by a Polarstar microplate reader (BMG Labtech). For fluorescent imaging, after the cells were treated with *a<sub>m</sub>*-ZnO@CuO@Au HNSs for 24 h and irradiated by 635 nm laser at different power densities (0 or 0.1 W/cm<sup>2</sup>) for 10 min, then incubated with DCFH-DA and DHE. The intracellular total ROS levels and the superoxide anion levels were determined by a fluorescent microscope at 485/515 and 485/585 nm, respectively,

after DCF and DHE staining.

**1.9 Hemolysis assay.** RBCs were isolated from freshly obtained ethylenediamine tetraacetic acid (EDTA)-stabilized rabbit blood by centrifuging and washing with PBS. Water and PBS were used as the positive and negative controls, respectively. Aliquots of 0.2 mL of diluted RBC suspension were added to 0.8 mL of PBS solutions containing different concentrations of RGD@*a<sub>m</sub>*-ZnO@CuO@Au@DOX HNSs. All the samples were mildly mixed and then tubes were kept standing at room temperature for 3 h and ready to rest, the absorbance of the upper supernatants was detected by UV-Vis spectroscopy at 540 nm [3].

**1.10 Morphological changes of RBCs.** RBCs were separated by centrifugation of whole rabbit blood at 1500 rpm for 10 min. The supernatant containing plasma and platelets was discarded. Washing was continued until the supernatant was clear. The RBC pellet was resuspended in 0.9% saline solution. The RGD@*a<sub>m</sub>*-ZnO@CuO@Au@DOX HNSs were diluted to the required concentration cell suspension. Observation of morphological changes by light microscopy were captured after 1.5 h of the RGD@*a<sub>m</sub>*-ZnO@CuO@Au@DOX HNSs exposure to analyze the morphological variation at the early stages of hemolysis. The obtained post-centrifugated pellet was diluted in 0.9% saline solution and mounted on clean glass slides covered with coverslips. The samples were then observed under Olympus BX41 microscope and photographed with an Olympus E-620 camera (Olympus Ltd., Japan).

**1.11 Cellular uptake and colocalization studies.** A549 cells were cultured in DEME medium containing 10% FBS and 1% penicillin/streptomycin at 37 °C in 5% CO<sub>2</sub>-humidified atmosphere. To determine the integrin binding affinity of RGD@*a<sub>m</sub>*-ZnO@CuO@Au@DOX HNSs, A549 tumor cells were incubated with RGD@*a<sub>m</sub>*-ZnO@CuO@Au@DOX HNSs (100 µg/mL), *a<sub>m</sub>*-ZnO@CuO@Au@DOX HNSs (100 µg/mL), and *a<sub>m</sub>*-ZnO@CuO@Au@DOX HNSs (100 µg/mL) in the

presence of cRGD (2  $\mu\text{g}/\text{mL}$ ) for 4 h. A549 cells were also incubated with RGD@ $a_m$ -ZnO@CuO@Au@DOX (100  $\mu\text{g}/\text{mL}$ ) for 4 h. For colocalization studies, A549 tumor cells were incubated with RGD@ $a_m$ -ZnO@CuO@Au@DOX HNSs (100  $\mu\text{g}/\text{mL}$ ) for 4 h and costained with Hoechst and Lyso-tracker green for another 20 min. Fluorescence imaging was performed with IX73 optical microscope (Olympus, Japan).

**1.12 Cytotoxicity analysis.** Cytotoxicity analysis of the composite was according to our previous study. For toxicity study,  $a_m$ -ZnO NPs were incubated with A549 cells for 48 h.

For  $\text{Zn}^{2+}/\text{Cu}^{2+}$  therapy/chemotherapy/PDT/PTT *in vitro*, A549 cells were incubated with DOX, RGD@ $a_m$ -ZnO@CuO@Au HNSs, RGD@ $a_m$ -ZnO@CuO@Au@DOX HNSs (200  $\mu\text{g}/\text{mL}$ ) for 4 h and then irradiated by 635 nm laser at different power densities (0, 0.1, and 2.0  $\text{W}/\text{cm}^2$ ) for 10 min. The cells were costained with calcein AM and propidium iodide (PI) for 30 min, washed with PBS, and then imaged by a laser scanning confocal microscope. MTT assay was carried out to determine cell viabilities under various conditions to further confirm the cytotoxicity and chemophototherapy efficacy of RGD@ $a_m$ -ZnO@CuO@Au@DOX HNSs. Cells were seeded into 96-well plates and incubated with different concentrations (0, 20, 50, 100, and 200  $\mu\text{g}/\text{mL}$ ) of RGD@ $a_m$ -ZnO@CuO@Au HNSs, RGD@ $a_m$ -ZnO@CuO@Au@DOX HNSs at 37 °C for 24 h in a humidified 5%  $\text{CO}_2$  atmosphere, each concentration of DOX, RGD@ $a_m$ -ZnO@CuO@Au HNSs, and RGD@ $a_m$ -ZnO@CuO@Au@DOX HNSs was carried out with six parallel groups. For *in vitro*  $\text{Zn}^{2+}/\text{Cu}^{2+}$  therapy, A549 cells were incubated with RGD@ $a_m$ -ZnO@CuO@Au@DOX HNSs (0, 20, 50, 100, and 200  $\mu\text{g}/\text{mL}$ ) at 37 °C for 4 h. For *in vitro*  $\text{Zn}^{2+}/\text{Cu}^{2+}$  therapy/chemotherapy, A549 cancer cells were incubated with RGD@ $a_m$ -ZnO@CuO@Au@DOX HNSs (0, 20, 50, 100, and 200  $\mu\text{g}/\text{mL}$ ) and free DOX, with same concentration of DOX at 37 °C for 4 h. For *in vitro*  $\text{Zn}^{2+}/\text{Cu}^{2+}$  therapy/chemotherapy/PDT, A549 cancer cells were incubated with

RGD@*a<sub>m</sub>*-ZnO@CuO@Au@DOX HNSs (0, 20, 50, 100, and 200 μg/mL) at 37 °C for 4 h under the same conditions and then irradiated by 635 nm laser (0 and 0.1 W/cm<sup>2</sup>) for 10 min. For *in vitro* Zn<sup>2+</sup>/Cu<sup>2+</sup> therapy/chemotherapy/PDT/PTT, A549 cells were incubated with RGD@*a<sub>m</sub>*-ZnO@CuO@Au@DOX HNSs (0, 100, and 200 μg/mL) at 37 °C for 4 h under the same conditions and then irradiated by 635 nm laser (2.0 W/cm<sup>2</sup>) for 10 min. After illumination, the cells were incubated for another 24 h. The culture medium was discarded, and 100 μL of dimethylsulfoxide was added. Absorbance was measured at 570 nm and was analyzed by the ANOVA method. The untreated cell population was used as the reference.

**1.13 Blood circulation.** All animal procedures were performed in accordance with the Guidelines for Care and Use of Laboratory Animals of Nanjing Normal University and approved by the Animal Ethics Committee of Nanjing Normal University. Female Kunming mice were used as animal models. 200 μL of RGD@*a<sub>m</sub>*-ZnO@CuO@Au@DOX HNSs was i.v. injected into three mice. At each time point, 20 μL of blood was collected from the mouse and then dissolved in 300 μL of lysis buffer (1% SDS, 1% Triton-100, 40 mM Tris acetate, 10 mM EDTA, and 10 mM DTT). To extract DOX from blood, 300 μL of HCl/isopropanol was added. Then, the mixture was incubated in dark overnight. By centrifuging to obtain the DOX in supernatant, the amount of DOX remaining in blood was determined by fluorescence.

**1.14 Mouse tumor model.** Nude female mice were obtained from Nanjing Biomedical Research Institute of Nanjing University. To establish lymph node metastasis models in female nude mice, A549 cells (1×10<sup>6</sup>) suspended in 100 μL PBS were injected subcutaneously into the each mouse. After about two weeks, the average size of tumor reached about 60 mm<sup>3</sup>.

**1.15 MR and fluorescence images.** RGD@*a<sub>m</sub>*-ZnO@CuO@Au@DOX HNSs dissolved in DI water with different concentrations were scanned by a 3.0 T clinical MRI scanner (BrukerBiospin Corporation, Billerica, MA, USA). T<sub>1</sub> weighted animal

MR imaging was performed under the same MR scanner with a special coil designed for small-animal imaging.

RGD@*a<sub>m</sub>*-ZnO@CuO@Au@DOX HNSs were intravenously injected into tumor bearing mice. Fluorescent scans were performed at various time points of post-injection (0, 2, 4, 6, 12, and 24 h) by a Maestro 2 Multispectral Small-animal Imaging System. The tumor-bearing mice were sacrificed by exsanguinations at 24 h post-injection, and the tumor and major organs were harvested.

### **1.16 *In vivo* toxicity, histological examination, and photothermal**

**effect.** First, the tumor-bearing mice were randomly divided into eight groups (n = 5, each group) and treated with PBS as control group, red light irradiation (635 nm, 0.1 or 2.0 W/cm<sup>2</sup>, 10 min), RGD@*a<sub>m</sub>*-ZnO@CuO@Au HNSs, DOX, RGD@*a<sub>m</sub>*-ZnO@CuO@Au@DOX HNSs, RGD@*a<sub>m</sub>*-ZnO@CuO@Au@DOX HNSs with red light irradiation (635 nm, 0.1 W/cm<sup>2</sup>, 10 min), and RGD@*a<sub>m</sub>*-ZnO@CuO@Au@DOX HNSs with red light irradiation (635 nm, 2.0 W/cm<sup>2</sup>, 10 min), respectively. It was noted that each mouse was injected 0.2 mL of samples (200 µg/mL) once every 2 d, and the tumor volumes and body weights of mice were recorded once every 2 d after treatment. After 14 d treatment, the typical organs (heart, liver, spleen, lung, and kidney) and tumor tissues of the mice in each group were dissected for further histology analysis. During the laser irradiation, the temperature profile and thermographic images were recorded by an infrared camera.

**1.17 Blood biochemical analysis.** The healthy male Kunming mice (body mass ca. 25 g) were provided by Nanjing Biomedical Research Institute of Nanjing University. The material dispersed in PBS (100 µL) at a total dose of 10 mg/kg was intravenously injected into the mice via the tail vein. Mice receiving the injection of only physiological saline were chosen as the control group. The mice in each group were sacrificed and the blood samples were separated from bodies to measure the blood biochemical indexes.

**1.18 Statistical analysis.** All quantitative data were represented by mean  $\pm$  SEM. The statistical significance between two groups and multiple groups was defined as  $P < 0.05$  by two-tailed student's t test or one-way ANOVA t-test. Two-way ANOVA analysis was performed when an additional factor or variant was involved in the experiment.

## 2. Supporting Figures

A special ZIF product with hierarchical morphology was obtained when the CTAC was added in the synthetic solution under any other identical conditions [2]. The growth of the ZIF could be described to a self-assembly process. The NPs had dandelion-like structure (spherical diameter ca. 580 nm) and composed of numerous radially nanorods as building blocks (Figure S1A). The nanorods, each 12 nm in length, were quite uniform (Figure S1A). EDS elemental maps indicated that Zn, C, and N were evenly distributed in the whole nanosphere (inset of Figure S1A). The XRD pattern shown in Figure S2 confirmed that the  $a_m$ -ZIF-90 NPs possessed a random network topology [1]. The Zn content in  $a_m$ -ZIF-90 NPs were 1.66 wt% from XPS measurement (Figure S1B). The metallic state of Zn was also confirmed via XPS (Figure S3). As shown in the previous paper [1], two N 1s peaks at 398.5 and 400.2 eV were found in the spectrum of the imidazole-2-carboxaldehyde molecule, which could be corresponded to imine and secondary amine groups, respectively. After the coordination with  $Zn^{2+}$ , the imine group disappeared, and a new peak at 399.3 eV was in favorable agreement with the tertiary amine (Figure S1C). A small part of the secondary amine group was observed due to the presence of free imidazole-2-carboxaldehyde linkers on the surface of NPs. The XPS spectra of both samples in C 1s and O 1s regions were nearly identical (Figure S4A,B). In light of these observations, the structure of  $a_m$ -ZIF-90 NPs is disordered in the presence of cetyltrimethylammonium chloride solution. CuNPs with an average size of  $3.1 \pm 0.4$  nm and AuNPs with an average size of  $3.2 \pm 0.8$  nm were introduced to  $a_m$ -ZIF-90 NPs via an *in situ* reduction method [4]. The CuNPs and AuNPs were formed not only on the external surface of  $a_m$ -ZIF-90 NPs but also across the entire structure of the  $a_m$ -ZIF-90 support owing its mesoporous nature, as shown in the TEM (Figure S1D) and HRTEM images (Figure S1E). Elemental analyses of these core-shell NPs through XPS (Figure S5) indicated that the core-shell particles contained Au, Zn, Cu, and O. Also, the metallic state of Cu, Zn, and Au was confirmed by XPS (Figure S6).

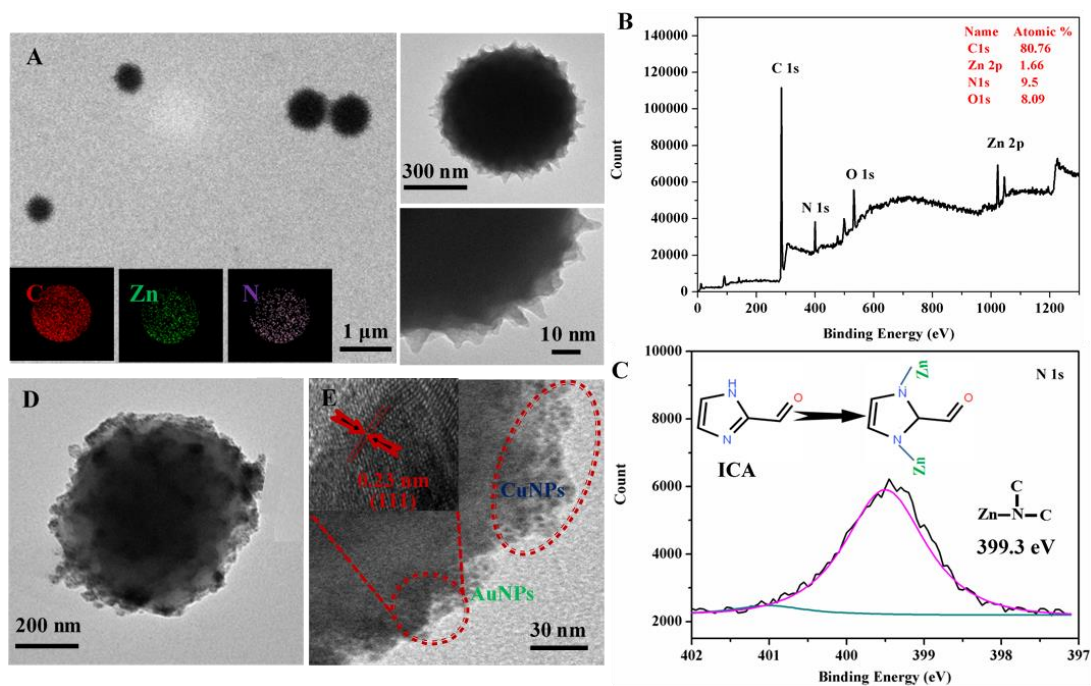


**Figure S1.** (A) TEM image of  $a_m$ -ZIF-90 NPs. Insert: TEM-EDS elemental mapping images of  $a_m$ -ZIF-90 NPs. (B) XPS survey spectrum of  $a_m$ -ZIF-90 NPs. (C) The high resolution N1s spectra of  $a_m$ -ZIF-90 NPs. (D) TEM (left) and (E) HRTEM (right) image of  $a_m$ -ZIF-90@Cu@Au NPs.

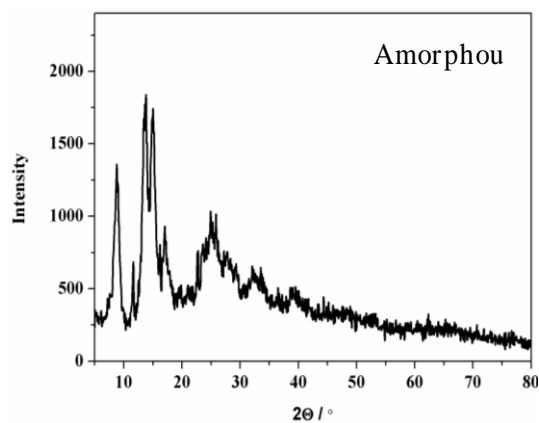


**Figure S2.** XRD patterns of  $a_m$ -ZIF-90 NPs.

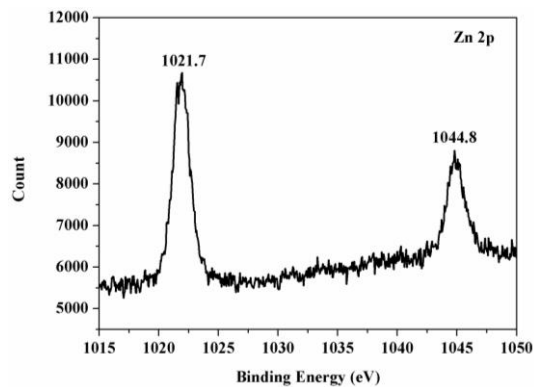


**Figure S3.** The high resolution Zn2p spectrum of  $a_m$ -ZIF-90 NPs.

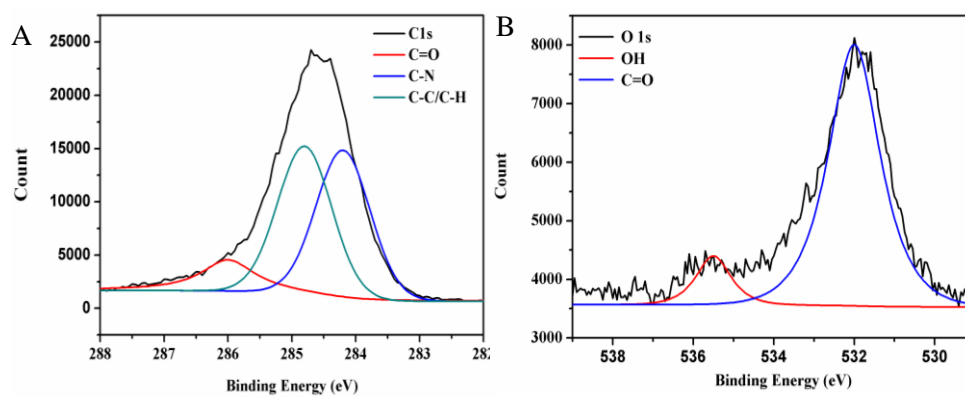


**Figure S4.** The high resolution (A) C1s and (B) O1s spectra of  $a_m$ -ZIF-90 NPs.

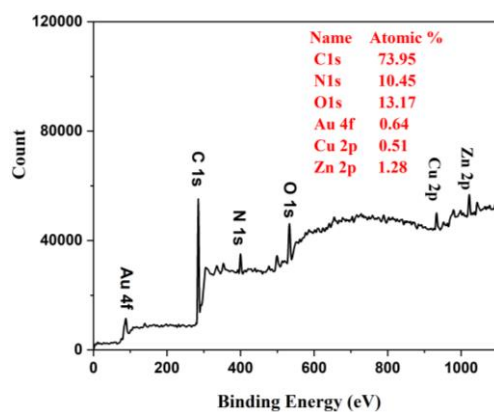


**Figure S5.** XPS survey spectrum of  $a_m$ -ZIF@Cu@Au NPs.

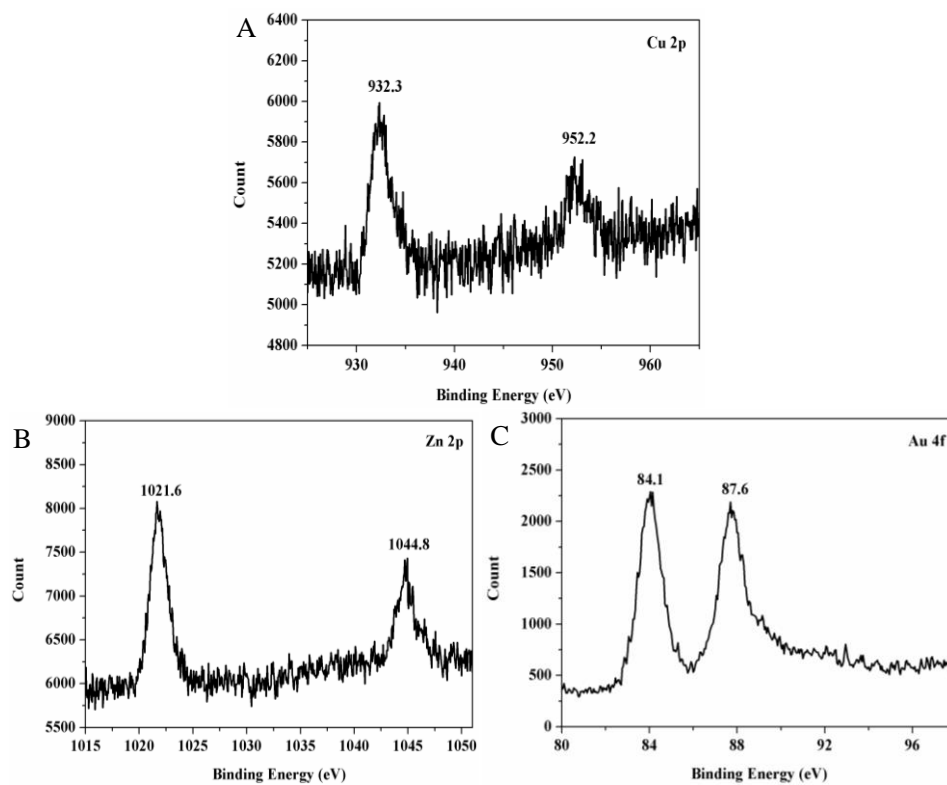


**Figure S6.** The high resolution (A) Cu2p, (B) Zn2p, and (C) Au4f spectra of  $a_m$ -ZIF@Cu@Au NPs.

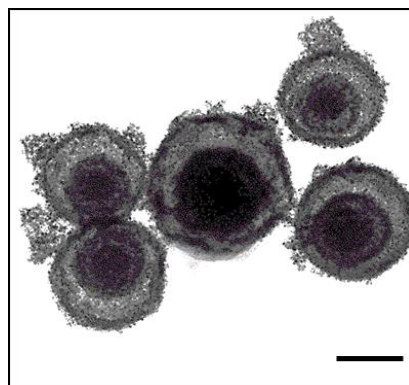


**Figure S7.** TEM image of  $a_m$ -ZnO@CuO@Au HNSs. Scale bar = 200 nm.

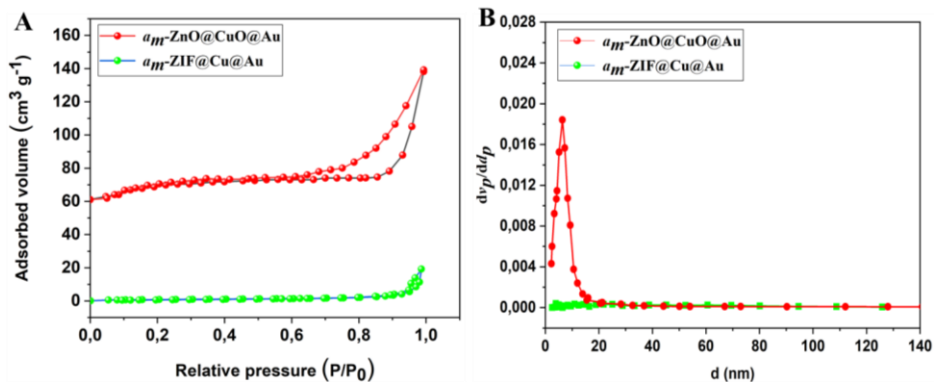


**Figure S8.** (A) Nitrogen sorption isotherms and (B) pore size distribution curves of *a<sub>m</sub>*-ZIF@Cu@Au NPs and *a<sub>m</sub>*-ZnO@CuO@Au NHSs.

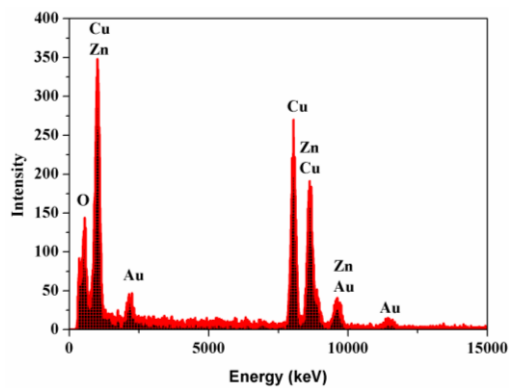


**Figure S9.** EDX spectrum of *a<sub>m</sub>*-ZnO@CuO@Au NHSs.

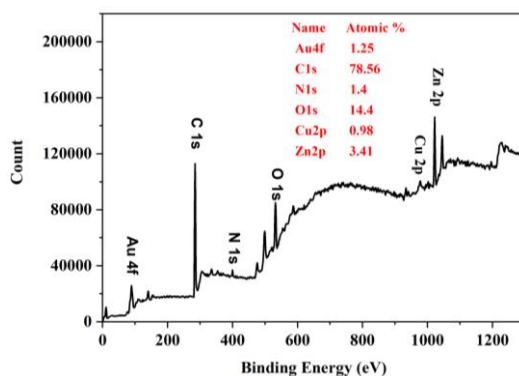


**Figure S10.** XPS survey spectrum of *a<sub>m</sub>*-ZnO@CuO@Au NHSs.

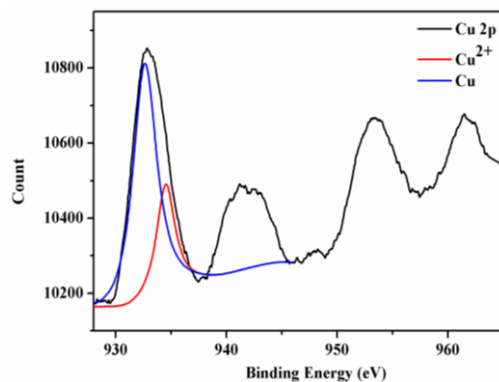


**Figure S11.** The high resolution Cu2p of  $a_m$ -ZnO@CuO@Au NHSs.

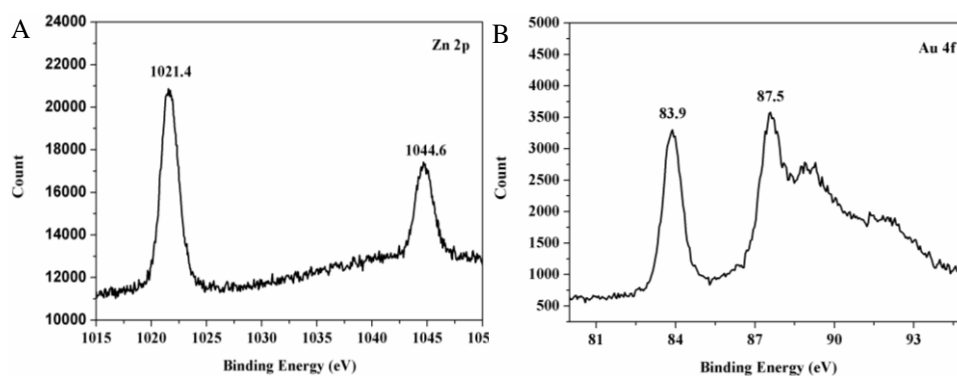


**Figure S12.** The high resolution (A) Zn2p and (B) Au4f of  $a_m$ -ZnO@CuO@Au NHSs.

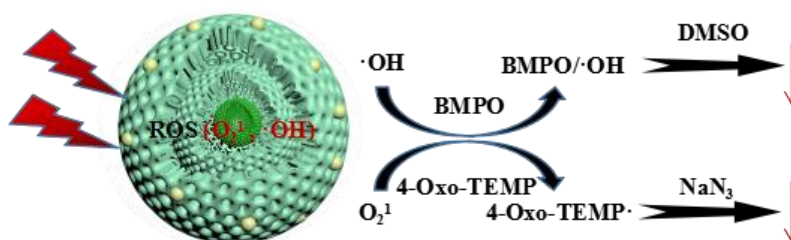


**Figure S13.** Methods used to distinguish the ROS and charge carriers formed during photoexcitation of  $a_m$ -ZnO@CuO@Au NHSs.

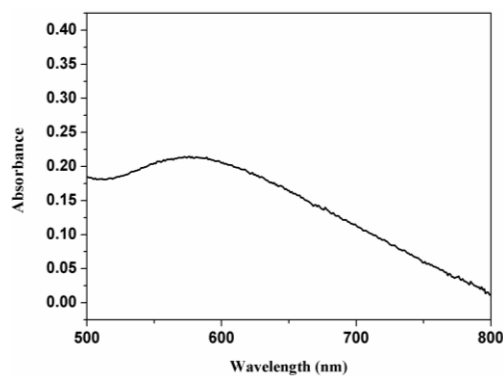


**Figure S14.** UV-vis absorption spectra of  $a_m$ -ZnO@CuO@Au NHSs.

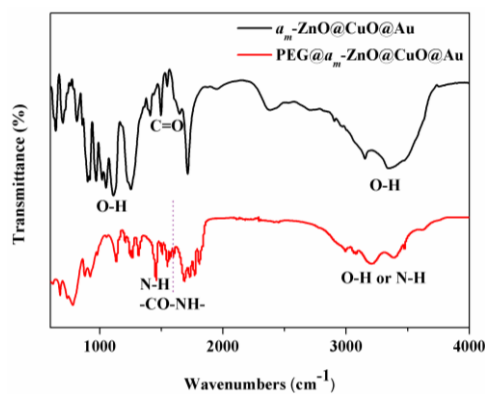


**Figure S15.** FT-IR spectrum of  $a_m$ -ZnO@CuO@Au NHSs and PEG@ $a_m$ -ZnO@CuO@Au NHSs.

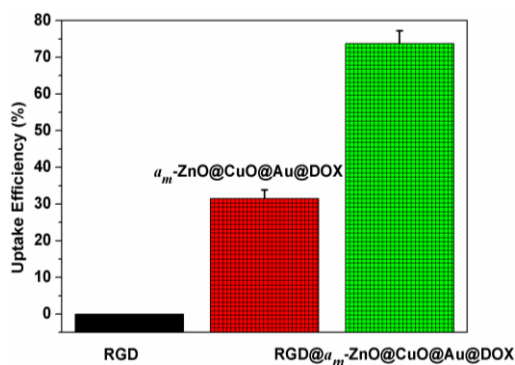


**Figure S16.** Cellular uptake efficiencies for cells after treatment with RGD,  $a_m$ -ZnO@CuO@Au NHSs, and RGD@ $a_m$ -ZnO@CuO@Au NHSs (each data point represents the mean value for  $n = 5$ ).

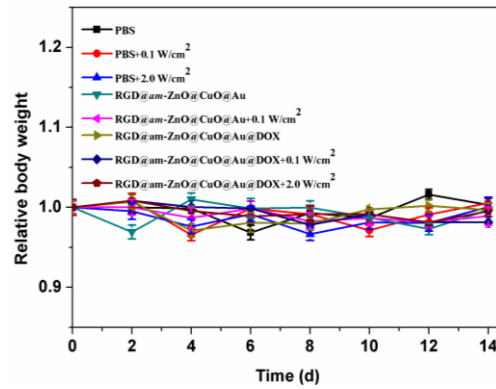


**Figure S17.** The body weights of mice were measured every other day.

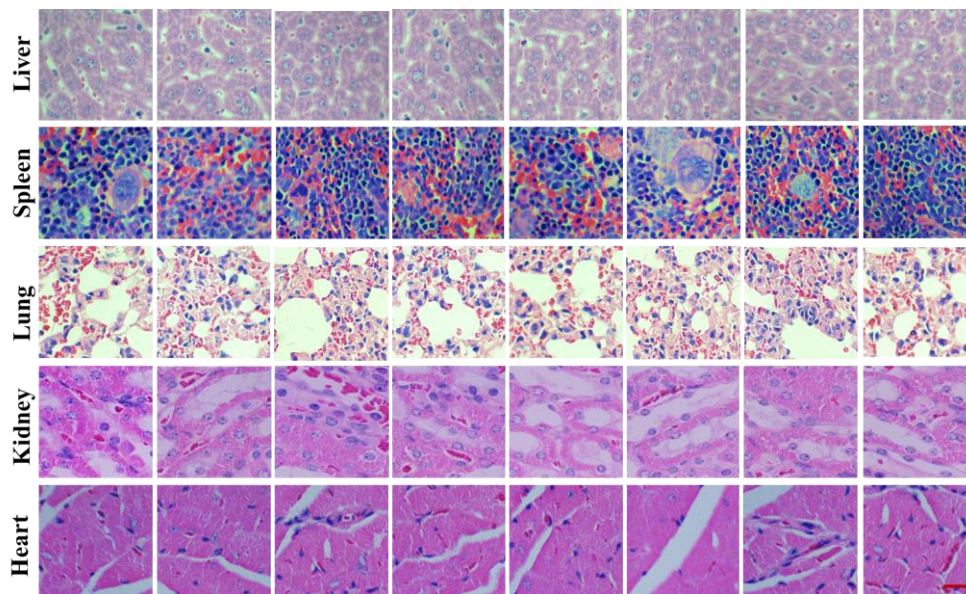


**Figure S18.** Histological data obtained from the liver, spleen, kidney, heart, and lung of the mice at 14 d treatment. The groups in the order from left to right: PBS, PBS+0.1 W/cm<sup>2</sup>, PBS+2.0 W/cm<sup>2</sup>, RGD@*a<sub>m</sub>*-ZnO@CuO@Au NHSs, RGD@*a<sub>m</sub>*-ZnO@CuO@Au NHSs+0.1 W/cm<sup>2</sup>, RGD@*a<sub>m</sub>*-ZnO@CuO@Au@DOX NHSs, RGD@*a<sub>m</sub>*-ZnO@CuO@Au@DOX NHSs+0.1 W/cm<sup>2</sup>, and RGD@*a<sub>m</sub>*-ZnO@CuO@Au@DOX NHSs+2.0 W/cm<sup>2</sup>. Scale bar = 50 μm.

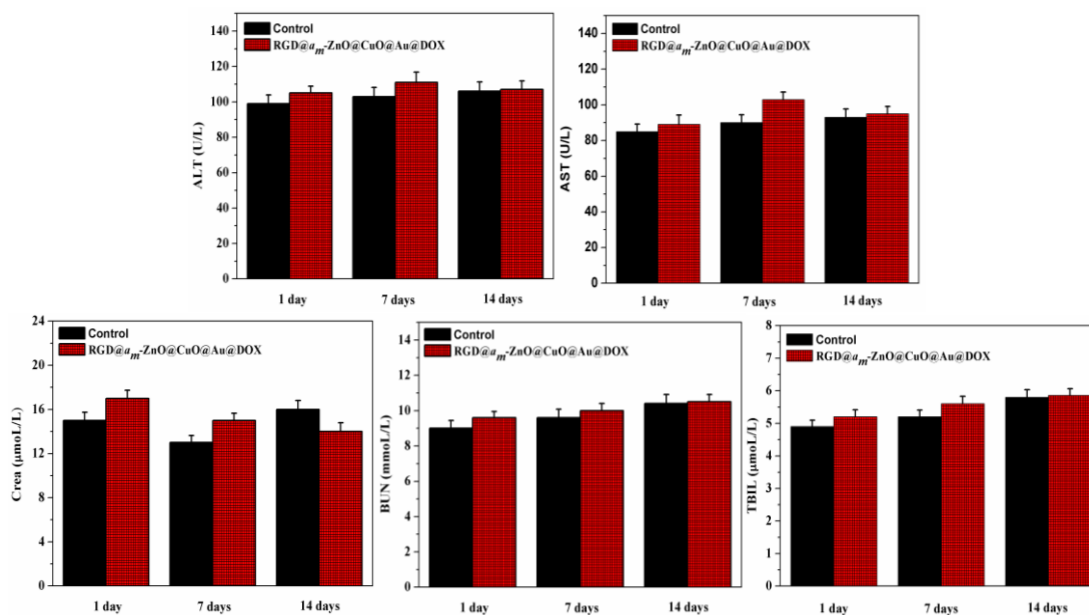


**Figure S19.** Serum biochemistry data for mice injected with PBS and RGD@a<sub>m</sub>-ZnO@CuO@Au@DOX NHSs (1, 7, and 14 days).

### 3. References

- [1] Zhan G, Zeng H C. A synthetic protocol for preparation of binary multi-shelled hollow spheres and their enhanced oxidation application. *Chemistry of Materials*, 2017, 29(23): 10104-10112.
- [2] Zhang M, Wang W, Wu F, et al. Magnetic and fluorescent carbon nanotubes for dual modal imaging and photothermal and chemo-therapy of cancer cells in living mice. *Carbon*, 2017, 123: 70-83.
- [3] Tan J, Meng N, Fan Y, et al. Hydroxypropyl-β-cyclodextrin–graphene oxide conjugates: Carriers for anti-cancer drugs. *Materials Science and Engineering: C*, 2016, 61: 681-687.
- [4] Cao, S.; Bennett, T. D.; Keen, D. A.; Goodwin, A. L.; Cheetham, A. K. Amorphization of the prototypical zeolitic imidazolate framework ZIF-8 by ball-milling. *Chemical Communications*. 2012, 48: 7805-7807.